

Imaging Molecular Structures by Electron Diffraction Using an Intense Few-Cycle Pulse

S. X. Hu* and L. A. Collins†

Theoretical Division, Los Alamos National Laboratory, Los Alamos, New Mexico 87545, USA
(Received 24 August 2004; published 24 February 2005)

As an intense few-cycle pulse interacts with an atomic or molecular target, its strong oscillating field may first pull electrons out of the target and subsequently drive them back to scatter on the target. The scattering may occur only a few times or even once during the interaction. This unique property of few-cycle pulses enables one to image ultrafast transient structures of matter by the means of pulse-driven electron diffraction. We demonstrated this phenomenon with K_2^+ via three-dimensional calculations of the time-dependent Schrödinger equation.

DOI: 10.1103/PhysRevLett.94.073004

PACS numbers: 33.80.Rv, 34.80.Bm, 34.80.Qb

Since its discovery in 1927 [1], electron diffraction has provided a powerful tool for imaging structures of matter. Most recently, ultrafast electron diffraction (UED) has proved essential for imaging transient events such as those encountered in chemical reactions [2] and in the melting of solids [3]. The electron pulses in conventional UED, which are generated from an external photocathode, have picosecond (ps) to subpicosecond widths for current third-generation apparatus [2]. The time resolution of an UED experiment is basically limited by this pulse width. However, minimizing the space-charge-induced broadening of the electron pulse requires a low electron flux, which in turn limits the sensitivity of UED. On the other hand, laser studies have demonstrated that an oscillating intense laser field can drive electrons of an atom or molecule back and forth through the target [4,5]. Essentially, these laser-driven electrons scatter from their “parent” targets, which, in fact, accounts for observations of high-energy plateaus in above-threshold-ionization (ATI) spectra [6] and non-sequential double ionization [7]. This observation led Zou, Bandrauk, and Corkum [8] to propose laser-induced electron diffraction (LIED) for momentum angular distribution measurements. Recent two-dimensional momentum studies of intense laser interactions with molecules have also indicated diffraction signatures in the ATI spectrum [9,10]. In contrast to the conventional UED, the LIED has its electron source extracted from the target itself, and the electron pulse can almost entirely scatter from the target, provided that the applied laser is linearly polarized. Besides the extremely ultrafast (femtoseconds) time resolution of LIED, the ultrahigh current density ($\sim 10^{10}$ A/cm² [11]) of intense laser-driven electron pulses can tremendously improve the sensitivity of electron diffraction. However, intense laser pulses have, in general, a width from 20 to 50 fs that contains about ten cycles within the envelope. In this case, the laser-induced electron diffraction may occur many times, thus limiting the observation of a clear diffraction pattern.

On the other hand, few-cycle pulses (FCPs) [12], so short that only a few (~ 2) optical oscillations exist within the pulse envelope, may serve as practical candidates for

LIED. In fact, the extreme case of FCPs, the so-called single-cycle pulse (SCP), has also been produced, though only weakly [13]. The generation of these extremely short pulses has therefore stimulated both experimental and theoretical studies of their interactions with matter [14] and raised the hope of doing electron diffraction with a few-cycle pulse. FCP-driven electron diffraction (FCP-DED), which happens only a few times or even once (SCP) within a pulse, might result in clear diffraction patterns. In this Letter, we demonstrate FCP-DED by numerically solving the three-dimensional (3D) time-dependent Schrödinger equation (TDSE) for a prototypical molecular ion exposed to intense FCPs. Exploring the detailed dynamics of FCP-DED, we gain insight into the molecular structure from the diffraction patterns.

To elucidate the FCP-driven electron diffraction, we investigate the representative case of a heavy molecular ion (K_2^+) interacting with such a pulse. The interaction scheme, shown in Fig. 1, consists of a K_2^+ molecule, aligned along the X axis [15] at a fixed internuclear distance R_c , and of a FCP, linearly polarized along the Z axis (i.e., vertical to the molecular axis). The potassium molecular ion with its single valence electron outside of a well-shielded core, closely resembles H_2^+ electronically so that we can employ a single active electron representation to model its interaction with the field. K_2^+ has other distinct advantages over H_2^+ . First, K_2^+ has a much longer vibrational period (~ 350 fs, compared to 7 fs), almost 2 orders

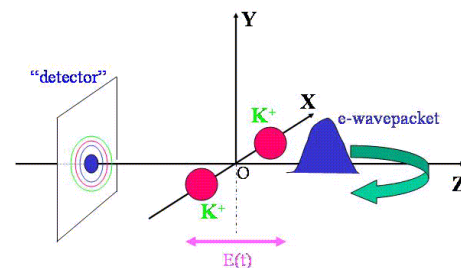


FIG. 1 (color online). The scheme of few-cycle-pulse-driven electron diffraction.

of magnitude longer than the applied FCP duration (2.7–5 fs), thus validating our fixed-nuclei approximation. Second, K_2^+ has a larger equilibrium internuclear distance ($R_c \sim 7.6$ bohr, compared to 1.4 bohr of H_2^+), which favors electron diffraction for interaction parameters accessible to current experiments. Third, the low ionization potential of K_2^+ ($I_p \sim 8$ eV), in contrast to that of H_2^+ ($I_p \sim 30$ eV), allows the use of moderate-intensity ($\sim 10^{14}$ W/cm²) FCPs. This significantly reduces our 3D computation efforts. The dynamics of the system is governed by the following 3D TDSE (atomic units are used throughout):

$$i \frac{\partial \Psi(x, y, z|t)}{\partial t} = \left[-\frac{1}{2} \nabla^2 - \frac{1}{a + \sqrt{(x + R_c/2)^2 + y^2 + z^2}} - \frac{1}{a + \sqrt{(x - R_c/2)^2 + y^2 + z^2}} + zE(t) \right] \Psi(x, y, z|t). \quad (1)$$

The dipole approximation is applied for the interaction term, where $E(t)$ represents the oscillating field of the FCP. To account for the inner electron screening effect, we use a 3D soft-Coulomb potential to describe the attractions of two nuclei [located at $(R_c/2, 0, 0)$ and $(-R_c/2, 0, 0)$] to the active electron, where $R_c = 7.6$ bohr is the equilibrium internuclear distance of K_2^+ . By adjusting the potential parameter a , we can obtain the ground state energy. Specifically, $a \approx 1.15$ gives the experimental ionization potential ($I_p \approx 8$ eV) of K_2^+ . The use of different soft-Coulomb potentials, for example, with the softening parameter “ a ” moved under the square root, had little effect on the diffraction patterns.

We evolved the 3D time-dependent wave function from the ground state of K_2^+ by using the real-space-product formula [16]. The parallel code was run with 60 CPUs on a SGI Origin2000 computer. An advanced absorptive mask function [17] was used at a range from the edges of each dimension, which guaranteed no reflection from the boundaries. We divided the total time propagation into a few time segments and moved our computing box of variable size to follow the probability density. By doing so instead of applying a larger constant-size box, we could afford the time-consuming calculations, yet still retain most of the probability within the calculation box. Typically, we employed a 3D box of the grid size varying from $500 \times 260 \times 260$ to $1500 \times 260 \times 260$ with a spatial step of $\Delta x = \Delta y = \Delta z = 0.198$ a.u. and a time step of $\Delta t \approx 0.04$ a.u. for the stable temporal propagation of the wave function.

We first studied the extreme case of FCPs, that is, a SCP interacting with K_2^+ . The SCP field is described by $E(t) = -E_0 \sin(\omega t)$, where E_0 is the field amplitude and ω stands for the laser frequency. The applied laser has an intensity of 10^{14} W/cm² and a wavelength of $\lambda = 800$ nm. The SCP duration is equal to $T \approx 2.7$ fs, and the system is freely evolved for an additional 2.3 fs. The detailed dynamics of

SCP-driven electron wave packets is indicated by Fig. 2, in which we plot the electron probability density [$P(x, z|t) = \int |\Psi(x, y, z|t)|^2 dy$] as a function of time. Such a single-cycle pulse can be viewed as two half-cycle pulses of opposite directions [18]. Under the interaction of the first half-cycle (negative) field, the electron wave packet is pulled out of the K_2^+ along the positive Z axis [see the first panel of Fig. 2 (at $t = 1.0$ fs)]. When the field flips its sign in the second half-cycle, the electron is first decelerated then stopped. Eventually, it moves back towards its parent K_2^+ . During this reversal, the field-driven electron wave packet develops quantum interferences that distinctly appear in Fig. 2 at $t = 2.5$ and 4.0 fs. These interference features are well known for intense laser-atom interactions [19,20]. After some time, most of the electron wave packet has returned to the vicinity of nuclei and begins to scatter away from the potential of K_2^+ in the absence of external fields (the SCP has already died off). We thus observe at $t = 5.0$ fs jets shooting at some angles to the negative Z axis (the last panel of Fig. 2), which could indicate electron diffraction.

To explore diffraction patterns, we must, as in the conventional UED experiments, determine the electron probability ($|\Psi(x, y, z = Z_0)|^2$) on a “detector” plane in XY , shifted a distance Z_0 away from the molecule (see Fig. 1). Although the diffraction pattern recorded in an experiment is the time integral of the electron probability at the detector, we observe that the pattern configuration hardly changes while its magnitude may vary from time to time. Thus, the snapshots, which we take at about the times when

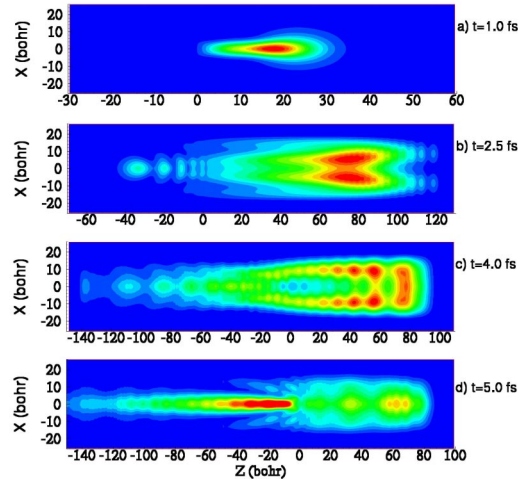


FIG. 2 (color online). The dynamics of SCP-driven electron diffraction, in which the electron probability density $P(x, z|t)$ is shown as a function of time. Those jets at the final stage of $t = 5.0$ fs are the evidence of SCP-driven electron diffraction. The single-cycle pulse has an intensity of 10^{14} W/cm², a wavelength at $\lambda = 800$ nm, and a duration of $T \approx 2.7$ fs. [Each panel has a total of 15 equal-spaced contour levels but in different ranges: (a) (3×10^{-4}) – (5×10^{-3}) , (b) (3.26×10^{-5}) – (4.88×10^{-4}) , (c) (1.62×10^{-5}) – (2.43×10^{-4}) , and (d) (2.05×10^{-5}) – (3.08×10^{-4}) .]

the large electron probability passes through the “detector plane,” should represent the dominant features of the diffraction pattern observed in the experiments. By placing such a detector plane at different positions Z_0 for the SCP-driven electron diffraction at $t = 5$ fs, we can demonstrate the change in the diffraction patterns from the near-zone (small Z_0) to the far-zone (large Z_0) region. The results are plotted in Figs. 3(a)–3(c) for $Z_0 = -27.62$, -39.5 , and -63.26 bohr, respectively. In the near-zone region Fig. 3(a) shows four diffraction spots surrounding the central bright one, with those perpendicular more intense than those parallel to the X axis. We recall that the molecular axis lies along the X direction. The two weak diffraction spots arise basically from the electron scattering from individual K^+ . Their intensity fades with an increasing detector distance from the molecule, as is seen in Figs. 3(b) and 3(c). The other two stronger diffraction spots originate from the constructive interference of scattering waves from both nuclei. Therefore, they carry the information of the molecular structure. Note that these spots will become a ring when averaging over molecular rotations in the XY plane.

The independent atom model (IAM) [21], which approximates the molecular scattering wave to be a superposition of waves from individual atoms, can pedagogically guide our understanding of the diffraction pattern formation. However, the IAM without any fitting does not give the quantitative results identical to those from our 3D simulations, since multiple scattering effects may play a role and the rescattered electron wave packet has been affected by early laser interactions.

Following the technique extensively used in the electron diffraction experiments [22], we can extract instantaneous molecular structure information from our calculated dif-

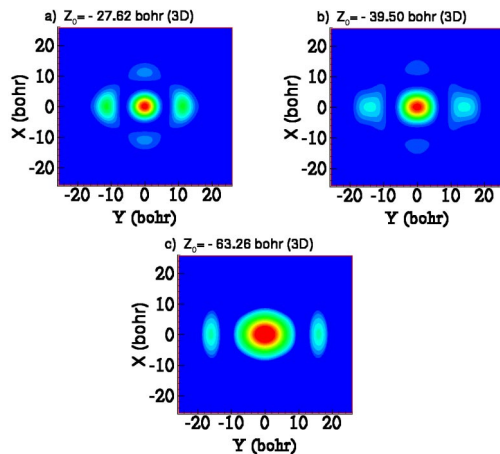


FIG. 3 (color online). The SCP-driven electron diffraction patterns, which are measured at different distances (from the molecule) (a) $Z_0 = -27.62$ bohr, (b) $Z_0 = -39.5$ bohr, and (c) $Z_0 = -63.26$ bohr. [Each panel has a total of 15 equal-spaced contour levels but in different ranges: (a) (1.89×10^{-6}) – (2.84×10^{-5}) , (b) (1.58×10^{-6}) – (2.37×10^{-5}) , and (c) (9.50×10^{-7}) – (1.37×10^{-5}) .]

fraction patterns. The procedure involves calculating the so-called radial distribution function $f(R)$, which is basically the Fourier transform of the generalized diffraction intensity [22]:

$$f(R) = \int s I(s) \times e^{isR} ds, \quad (2)$$

where the momentum transfer $s = 2k \sin(\theta/2)$ for elastic scattering and $I(s)$ is the diffraction intensity as a function of s . With this recipe, we compute the radial distribution function from our calculated diffraction pattern at $Z_0 = -63.26$ bohr [Fig. 3(c)], by taking $I(s) \propto |\Psi(x=0, y, z=Z_0)|^2$. The resulting radial distribution $f(R)$ is plotted (black solid line) as a function of the internuclear distance R in Fig. 4. The final result is obtained by averaging the returned electron momentum k over a width of $\delta k = 0.5$ a.u. centered at $k_0 \sim 1.0$ a.u. (determined from the interaction parameters considered), with a Gaussian distribution [23]. In Fig. 4 the black curve shows a peak located at $R = 7.67$ bohr that agrees very well with our “input” internuclear distance $R_c = 7.6$ bohr (indicated by the vertical black dashed line) for the TDSE calculation. The broad width of the peak is attributed to our limited-size detector (i.e., the XY plane size), which records only the first-order diffraction pattern. In experiments more fringes can be recorded so that their Fourier transform will result in a sharp peak for diatomic molecules. In addition to the equilibrium case of $R_c = 7.6$ bohr, we have also calculated the SCP-driven electron diffractions for other internuclear distance of $R_c = 5.0$ and 10.0 bohr. Similar diffraction patterns are obtained, from which the molecular structure information is generally derived. As an example, the radial distribution $f(R)$ for the case of $R_c = 10.0$ bohr is drawn with the right curve (red) in Fig. 4. It shows the peak position at $R = 9.84$ bohr in good agreement with $R_c = 10.0$ bohr. Once in the far zone, we observe little sensitivity of the extracted value of R to the choice of Z_0 .

Finally, we investigate the FCP-driven electron diffraction with the same molecular ion K_2^+ and design the FCP to put the initially bound electron through the same general evolution experienced with the SCP. A representative FCP

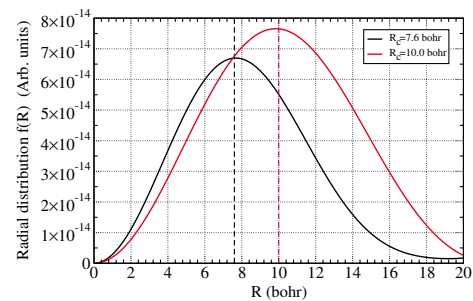


FIG. 4 (color online). The radial distribution evaluated by Fourier transform of the calculated electron diffraction patterns. The peak positions give the internuclear distances of molecules being imaged.

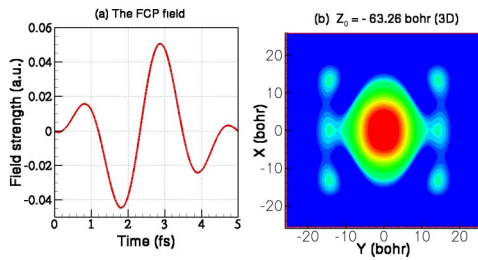


FIG. 5 (color online). (a) FCP electric field, and (b) the FCP-driven electron diffraction pattern shown at a distance $Z_0 = -63.26$ bohr. The few-cycle pulse has a duration of $T = 5$ fs, and other field parameters are the same as those used in Fig. 2.

field [24], shown in Fig. 5(a), derives from a vector potential, $A(t) = A_0 \sin^2(\pi t/T) \times \cos(\omega t + \phi)$, with the absolute phase $\phi = 230^\circ$ and pulse duration $T = 5$ fs. The other laser parameters are the same as those used in Fig. 2. The packet is then further propagated for another 2 fs, and the resulting far-zone diffraction pattern at $Z_0 = -63.26$ bohr displayed in Fig. 5(b). Since the FCP has field oscillations (though weak) other than the dominant single cycle, the FCP-driven electron diffraction has more interference structures. We clearly find two additional side peaks around the main diffracted peak. Basically, they can be attributed to the extra structures in the energy and spatial distribution of FCP-driven back electron wave packets. Nevertheless, the main features seen in the SCP-driven electron diffraction are still exhibited in Fig. 5(b). Taking into account the FCP field configuration (which determines the momentum distribution of the returned electron wave packets), we computed, using the diffraction pattern of Fig. 5(b), the radial distribution function. The resulting peak at $R = 7.84$ bohr is still within $\sim 3\%$ of the exact value $R_c = 7.6$ bohr.

In conclusion, we have elucidated the few-cycle pulse-driven electron diffraction through solving the fully three-dimensional TDSE. From diffraction patterns we can extract molecular structure information. Although we used intense FCPs for demonstrations, the concept of ultrashort pulse-driven electron diffraction can be realized with moderately strong (10^8 – 10^{12} W/cm²) few-cycle pulses. For example, one may first attach an electron to a target, then apply FCPs of certain intensities to drive the attached (weakly bounded) electron to diffract on the target, thereby gaining the structural information of neutral targets.

This work was performed under the auspices of the U.S. Department of Energy through the Los Alamos National Laboratory under the LDRD-PRD program.

*Electronic address: suxing@lanl.gov

†Electronic address: lac@lanl.gov

[1] *Electron Diffraction, 1927–1977*, edited by P. J. Dobson, J. B. Pendry, and C. J. Humphreys, Institute of Physics

Conference Series No. 41 (Institute of Physics, Bristol, U.K., 1977), 0305-2346.

- [2] H. Ihee *et al.*, *Science* **291**, 458 (2001).
 [3] B. J. Siwick *et al.*, *Science* **302**, 1382 (2003).
 [4] P. B. Corkum, *Phys. Rev. Lett.* **71**, 1994 (1993).
 [5] K. C. Kulander, K. J. Schafer, and J. L. Krause, in *Super-Intense Laser-Atom Physics*, NATO Advanced Study Institute, Ser. B, Vol. 316 (Plenum, New York, 1993), p. 95.
 [6] G. G. Paulus *et al.*, *Phys. Rev. Lett.* **72**, 2851 (1994); G. G. Paulus *et al.*, *J. Phys. B* **27**, L703 (1994); M. V. Frolov *et al.*, *Phys. Rev. Lett.* **91**, 053003 (2003).
 [7] B. Walker *et al.*, *Phys. Rev. Lett.* **73**, 1227 (1994); R. Kopold *et al.*, *Phys. Rev. Lett.* **85**, 3781 (2000); G. L. Kamta and A. F. Starace, *Phys. Rev. Lett.* **86**, 5687 (2001).
 [8] T. Zou, A. D. Bandrauk, and P. B. Corkum, *Chem. Phys. Lett.* **259**, 313 (1996).
 [9] M. Lein, J. P. Marangos, and P. L. Knight, *Phys. Rev. A* **66**, 051404(R) (2002).
 [10] M. Spanner *et al.*, *J. Phys. B* **37**, L243 (2004).
 [11] H. Nilkura *et al.*, *Nature (London)* **417**, 917 (2002); **421**, 826 (2003).
 [12] M. Nisoli *et al.*, *Opt. Lett.* **22**, 522 (1997); T. Brabec and F. Krausz, *Rev. Mod. Phys.* **72**, 545 (2000), and references therein.
 [13] O. Albert and G. Mourou, *Appl. Phys. B* **69**, 207 (1999); M. Spanner *et al.*, *Opt. Lett.* **28**, 749 (2003); A. V. Sokolov, *Appl. Phys. B* **77**, 343 (2003).
 [14] A. de Bohan *et al.*, *Phys. Rev. Lett.* **81**, 1837 (1998); G. G. Paulus *et al.*, *Nature (London)* **414**, 182 (2001); D. B. Milošević, G. G. Paulus, and W. Becker, *Phys. Rev. Lett.* **89**, 153001 (2002); G. L. Kamta and A. F. Starace, *Phys. Rev. A* **68**, 043413 (2003); J. Zhang and Z. Z. Xu, *Phys. Rev. A* **68**, 013402 (2003); S. X. Hu and L. A. Collins, *Phys. Rev. A* **70**, 013407 (2004); **70**, 035401 (2004); A. Gurtler *et al.*, *Phys. Rev. Lett.* **92**, 033002 (2004).
 [15] H. Stapelfeldt and T. Seideman, *Rev. Mod. Phys.* **75**, 543 (2003), and references therein.
 [16] L. A. Collins, J. D. Kress, and R. B. Walker, *Comput. Phys. Commun.* **114**, 15 (1998).
 [17] A. N. Hussain and G. Roberts, *Phys. Rev. A* **63**, 012703 (2000).
 [18] S. X. Hu and A. F. Starace, *Phys. Rev. A* **68**, 043407 (2003).
 [19] H. G. Muller and F. C. Kooiman, *Phys. Rev. Lett.* **81**, 1207 (1998).
 [20] M. Protopapas *et al.*, *Phys. Rev. A* **53**, R2933 (1996); J. Prager and C. H. Keitel, *J. Phys. B* **35**, L167 (2002).
 [21] M. Ben-Nun, J. Cao, and K. R. Wilson, *J. Phys. Chem. A* **101**, 8743 (1997).
 [22] *Stereochemical Applications of Gas-Phase Electron Diffraction*, edited by I. Hargittai and M. Hargittai (VCH, New York, 1988), and references therein.
 [23] R. Grobe and M. V. Fedorov, *J. Phys. B* **26**, 1181 (1993); B. Gottlieb *et al.*, *Phys. Rev. A* **54**, R1022 (1996).
 [24] A. Baltuska, T. Fuji, and T. Kobayashi, *Phys. Rev. Lett.* **88**, 133901 (2002); G. G. Paulus *et al.*, *Phys. Rev. Lett.* **91**, 253004 (2003); A. Apolonski *et al.*, *Phys. Rev. Lett.* **92**, 073902 (2004).